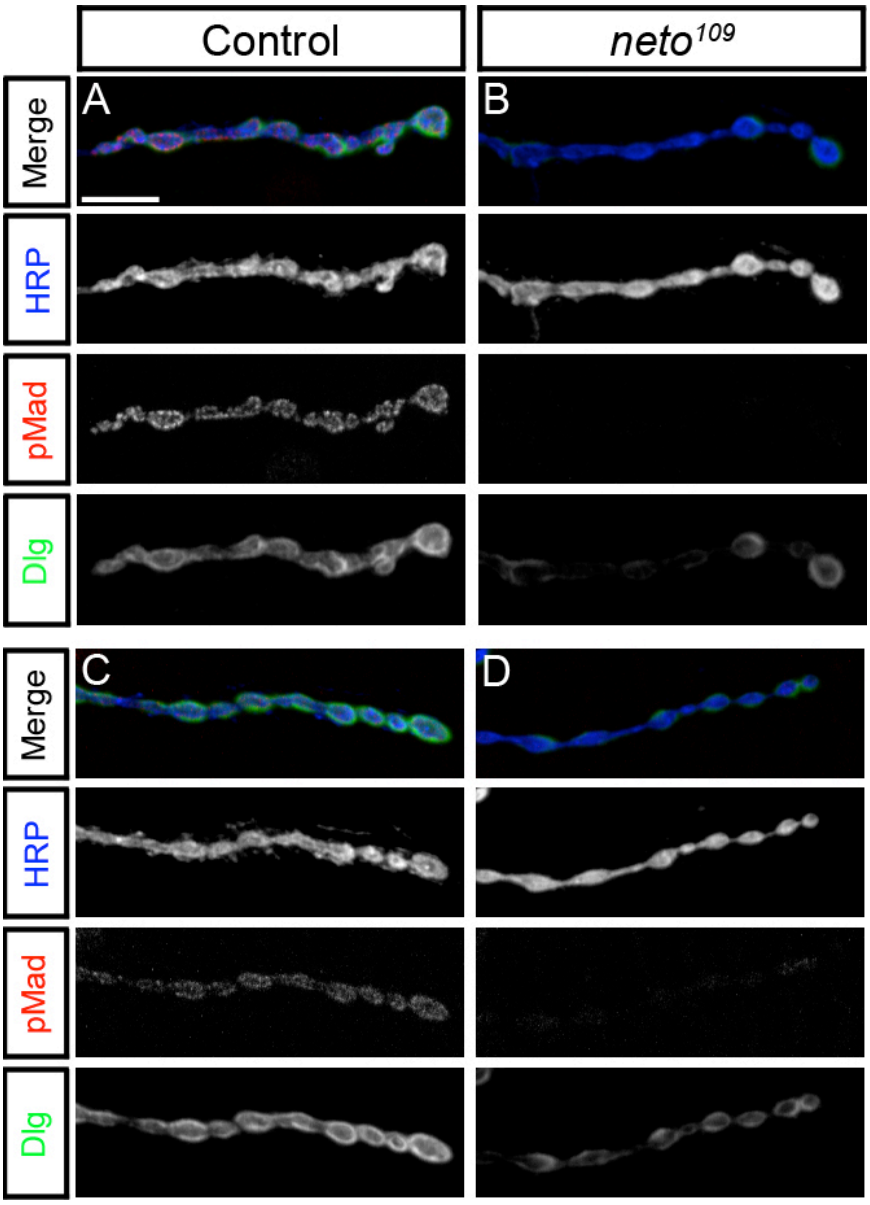


**Fig. S1: Multiple antibodies reveal loss of pMad in *neto* hypomorphs.**
Immunostaining with anti-pMad antibodies from Peluso et al. 2011 (A,B) or Smith et. al 2012 (C,D).
Scale bars: 10 μm.
Genotypes: (A,C) Precise excision; (B,D) *neto*$^{109}$.

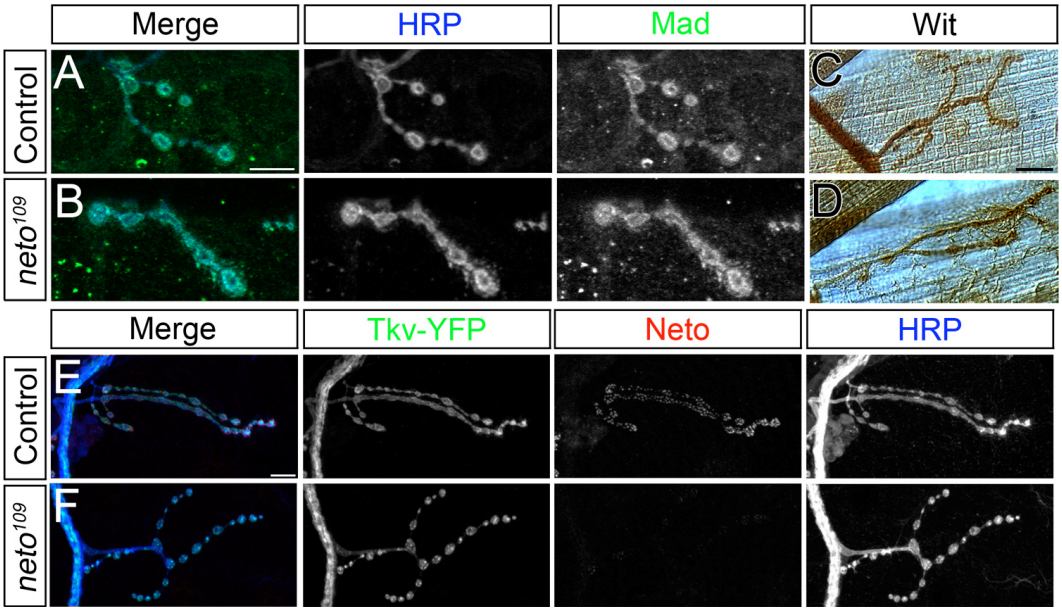


**Fig. S2. BMP pathway components appear normally expressed in *neto*$^{109}$ NMJ.**
Immunostaining with anti-Mad (A-B) or anti-Wit (C-D) antibodies in *neto*$^{109}$ resembles control animals. Thickveins-YFP expressed in motor neurons of *neto*$^{109}$ localizes to the NMJ similar to control animals (E-F).
Scale bars: 10 μm.
Genotypes: (A,C,E) Precise excision; (B,D,F) *neto*$^{109}$.

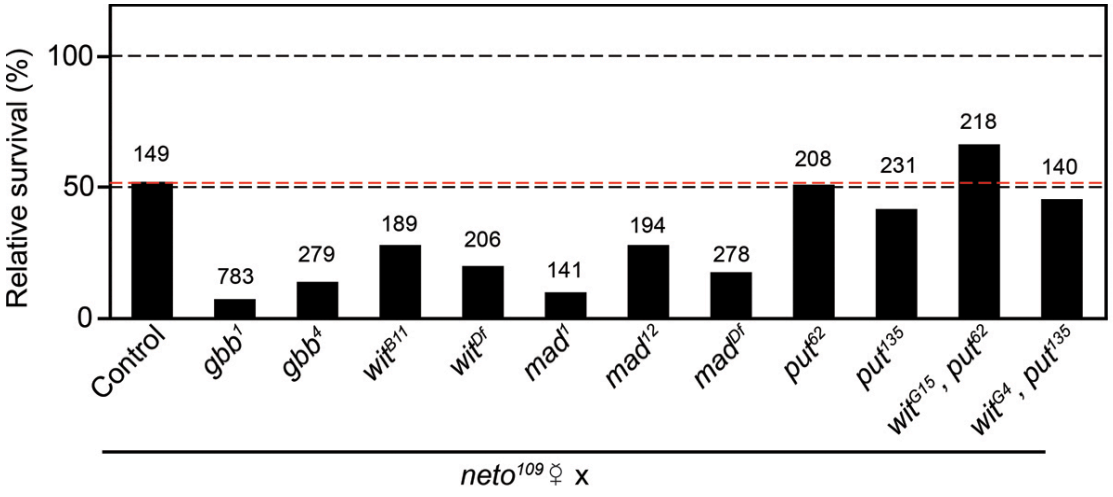


**Fig. S3. Simultaneous loss of Neto and BMP pathway components causes synthetic lethality.**
Hypomorphic *neto*$^{109}$ virgins were crossed with males bearing mutations in various BMP pathway genes. We counted the F1 progenies and compared the numbers of hemizygous males (*neto*$^{109}$/*Y* ; *mutant*/ +) and transheterozygous females (*neto*$^{109}$/ + ; *mutant*/ +). In the absence of any additional mutations in BMP pathway components, 52% of *neto*$^{109}$/*Y* males (relative to *neto*$^{109}$/+ females) survive to adulthood. Removal of one copy of BMP pathway components in this background increases the *neto*$^{109}$/*Y* lethality further. Numbers on top of the bars indicate total number of adults (males plus females) counted for each condition.

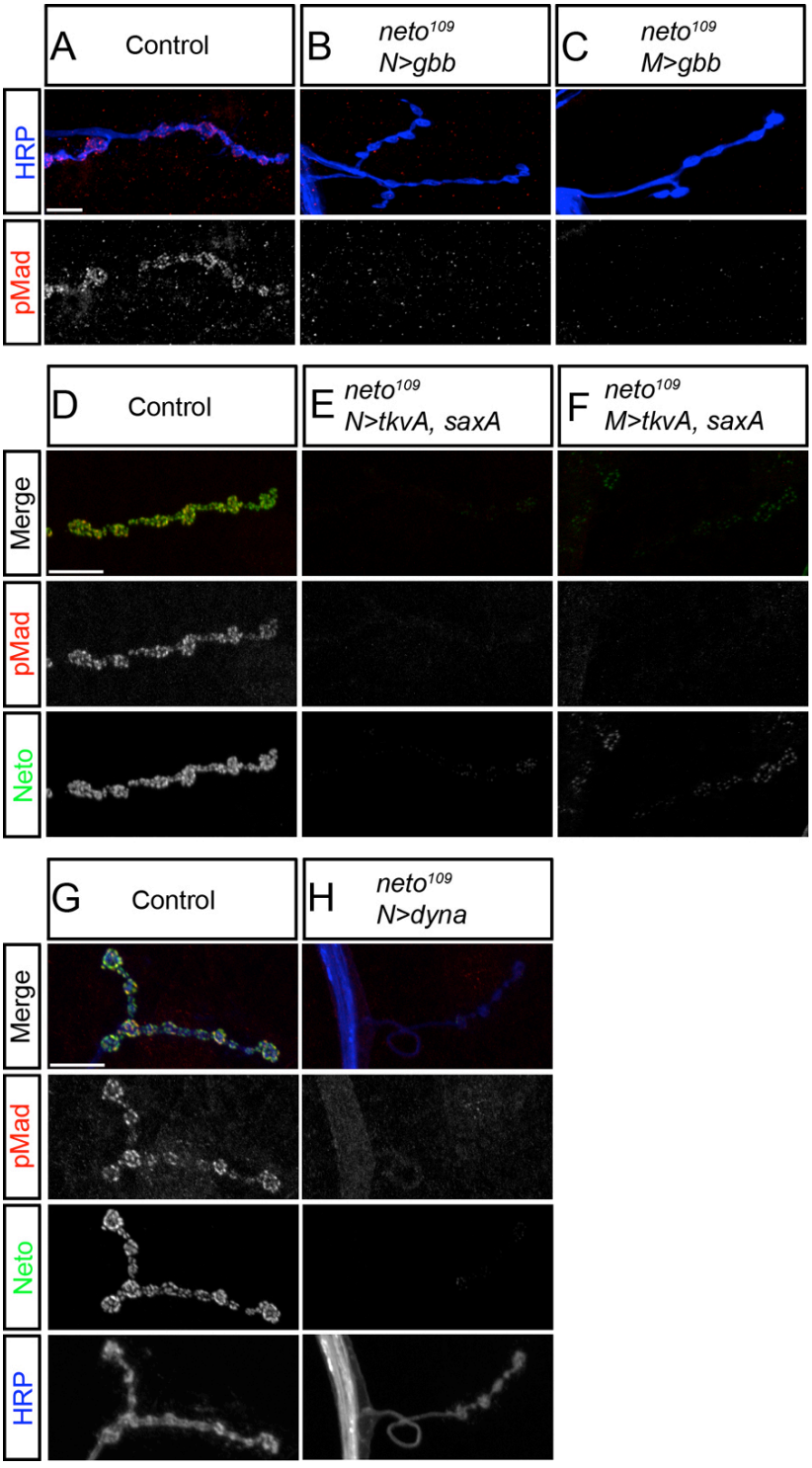


**Fig. S4. Loss of synaptic pMad in *neto* hypomorphs cannot be reversed by increased BMP signaling.**

(A-C) Overexpression of *gbb* in neurons (B) or muscles (C) cannot restore synaptic pMad in *neto* hypomorphs. (D-F) Overactivation of type-I BMP receptors, Sax and Tkv, in neurons (E) or muscles (F) cannot restore the synaptic pMad levels in *neto* hypomorphs. (G-H) Overexpression of *dynamitin* (*dyna*) in $neto^{109}$ neurons cannot rescue synaptic pMad. Scale bars: 10 μm.

Genotypes: (A, D, G) Precise excision; (B) $neto^{109}$, *380-Gal4; UAS-gbb9.9*; (C) $neto^{109}$; *G14-Gal4/UASgbb9.9;* (E) $neto^{109}$, *380-Gal4; +; UAS-tkv*$^{Q253D}$, *UAS-sax*$^{Q263D}$; (F) $neto^{109}$; *G14-Gal4/+; UAS-tkv*$^{Q253D}$,*UAS-sax*$^{Q263D}$

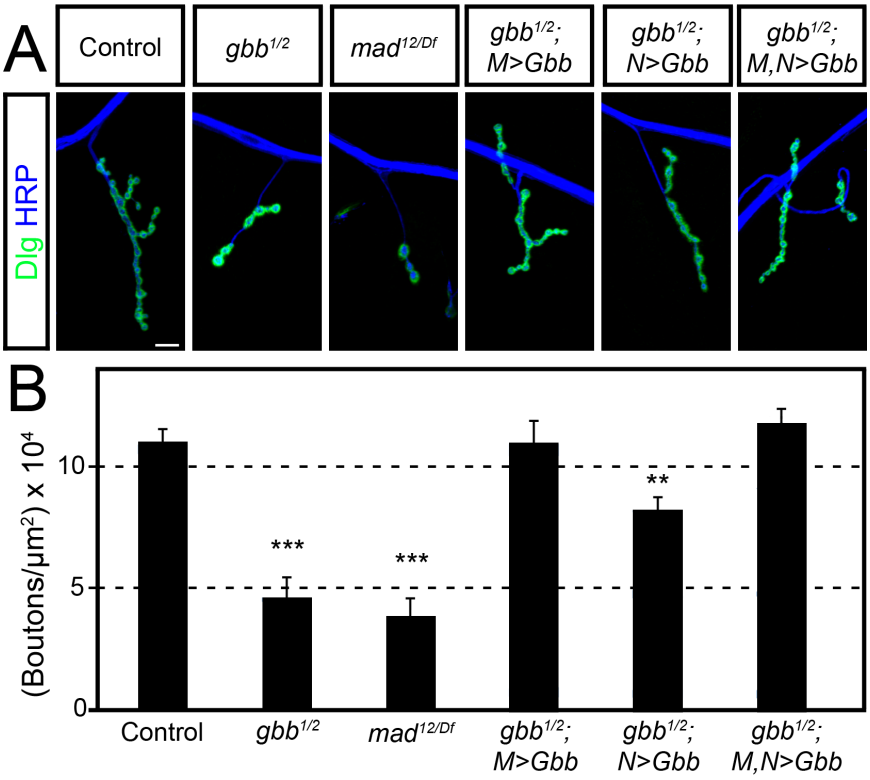


**Fig. S5. Muscle expression of *UAS-gbb* rescues the growth phenotype of *gbb* mutants.**

(A) Representative confocal images of muscle 4 NMJ, abdominal segment 3, in third instar larvae immunostained against Dlg (Green) and HRP (Blue). (B) Quantification of mean number of type IB boutons per µm$^2$ (muscle 4, abdominal segment 3). At least ten segments were analyzed per genotype. Error bars represent SEM. ** $p < 0.005$; *** $p < 0.001$ compared to control.

Scale bar: 10 µm

Genotypes: control (precise excision); *gbb$^{1/2}$* (*gbb$^{1}$/gbb$^{2}$*), *mad$^{12}$/$^{Df}$* (*mad$^{12}$/ Df(2L)C28*), *gbb$^{1/2}$; M>Gbb* (*gbb$^{1}$/gbb$^{2}$,UASgbb$^{9.9}$; 24B-Gal4/+*), *gbb$^{1/2}$; N>Gbb* (*gbb$^{1}$/gbb$^{2}$,UASgbb$^{9.9}$; elav-Gal4/+*), *gbb$^{1/2}$; M,N>Gbb* (*gbb$^{1}$/gbb$^{2}$,UASgbb$^{9.9}$; elav-Gal4, 24B-Gal4/+*)

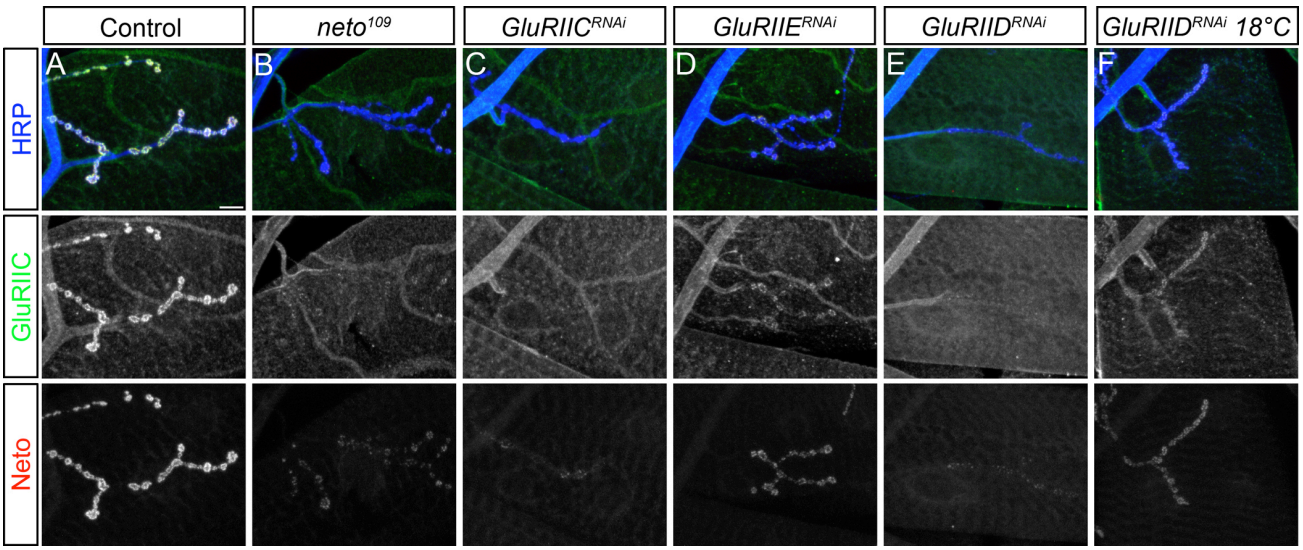


**Fig. S6. Genetic manipulation of *iGluR* levels via *RNAi*.**
Compared with control (A) or *neto*$^{109}$ (B), *RNAi*- mediated depletion of the *GluRIIC* subunit produces moderate reduction of iGluRs clusters (C), depletion of the *GluRIIE* subunit has a weak defect (D), and depletion of the *GluRIID* subunit induces a severe loss of iGluRs (E). Rearing *GluRIID*$^{RNAi}$ animals at 18°C partially preserves the iGluR clusters (F).
Scale bars: 10 μm.
Genotypes: (A) Precise excision; (B) *neto*$^{109}$; (C) *G14-Gal4/+; UAS-GluRIIC*$^{RNAi}$/+; (D) *G14-Gal4/+;UAS-GluRIIE*$^{RNAi}$/+; (E, F) *G14-Gal4/+; UAS-GluRIID*$^{RNAi}$/+.

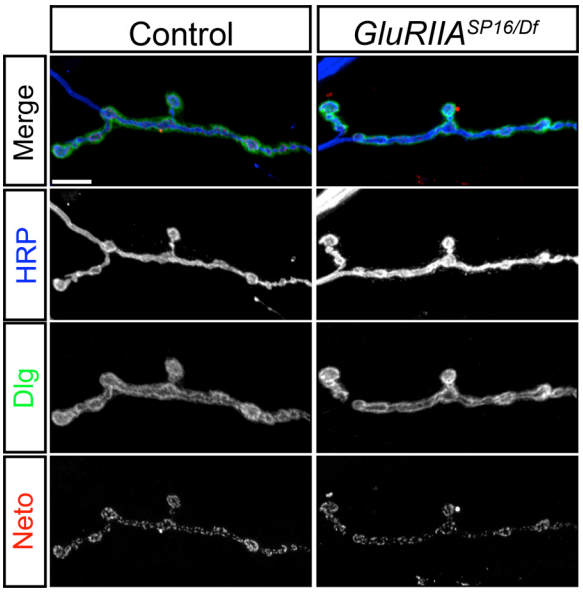


**Fig. S7. Postsynaptic components cluster normally in *GluRIIA* mutants.**
Immunostaining against Dlg and Neto appears similar in *GluRIIA* mutants compared to control animals.
Scale bars: 10 μm.
Genotypes: control (precise excision); *GluRIIA*$^{SP16/Df}$ (*GluRIIA*$^{SP16}$/*Df(2L)clh4)*

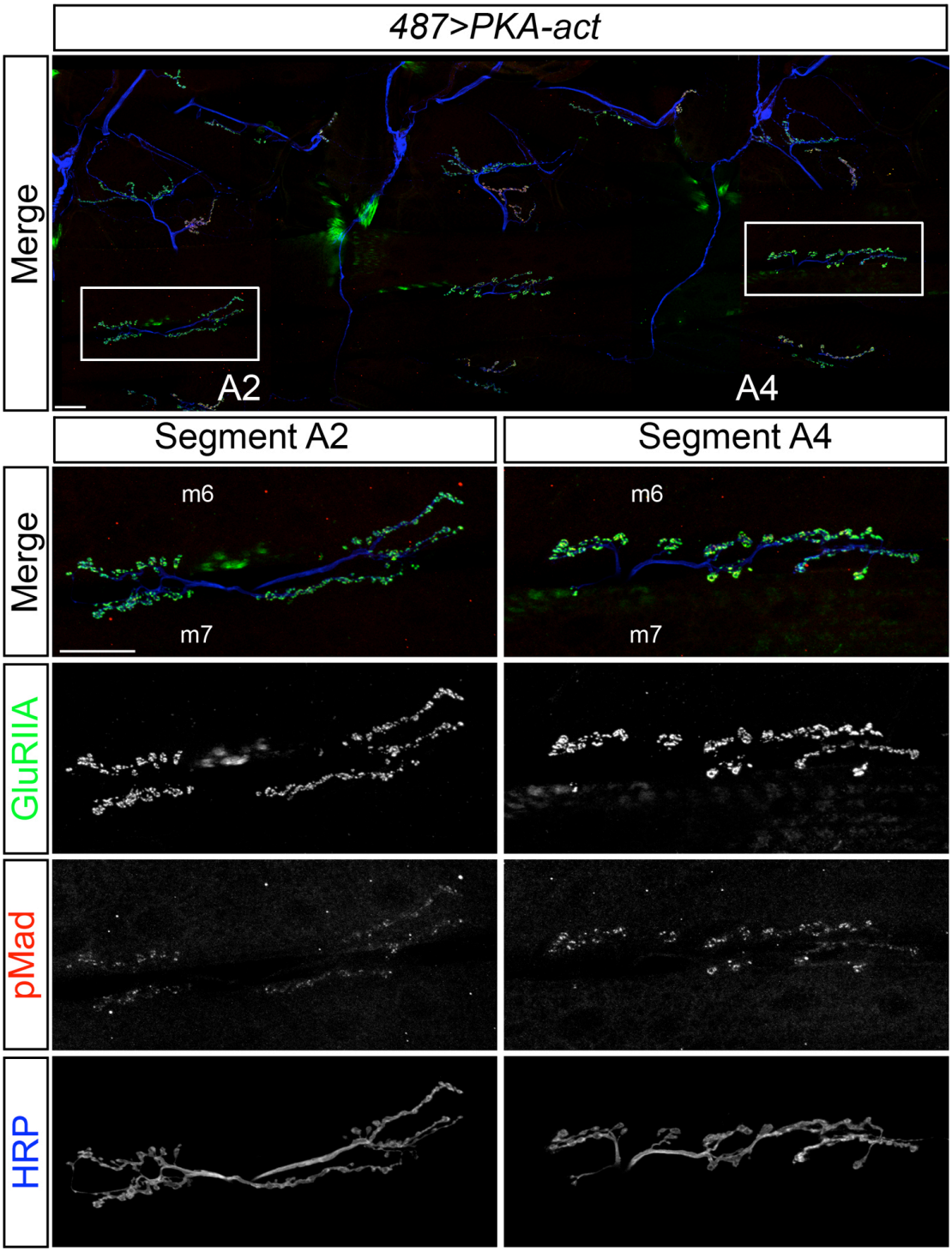


**Fig. S8. Synaptic pMad accumulation follows the activity gradient of type-A receptors.**

Confocal images of third instar larvae body wall muscle, abdominal segments A2-A4, stained with anti-GluRIIA antibodies (green), anti-pMad (red), and anti-HRP (blue). PKA activity follows the gradient of *BG487-Gal4* expression: high levels anteriorly and low levels towards the posterior side. Synaptic pMad is strongly inhibited in A2 (at high levels of PKA expression/ low receptor activity), and it is mildly reduced in A4 (at low levels of PKA expression/ high receptor activity).

Scale bars: 30 μm.

Genotype: *487>PKA$^{act}$* (*BG487-Gal4/UAS-PKA.mC*)

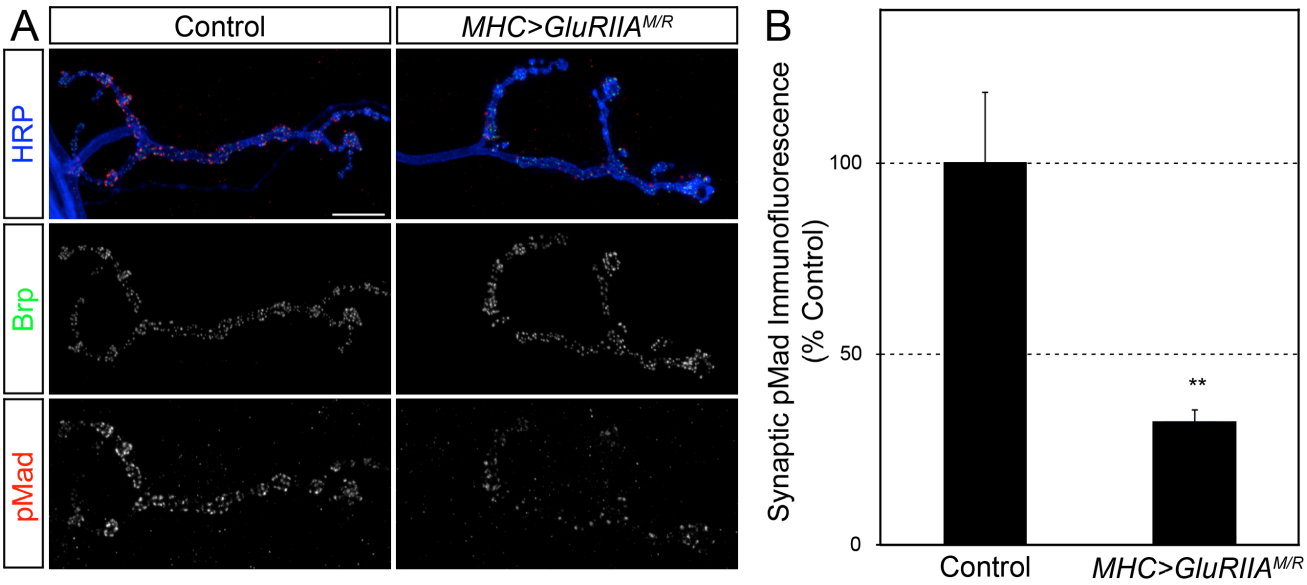


**Figure S9. Synaptic pMad decreases when a non-functional *GluRIIA* is expressed in the muscle.**

(A) Confocal images for muscle 4 NMJ on abdominal segment 3 stained for HRP (blue), Brp (green), and pMad (red). Synaptic pMad is reduced when a non-functional GluRIIA is expressed in muscles. (B) Quantification of synaptic pMad in animals expressing *GluRIIA*$^{M/R}$ in the muscle. Ten segments were analyzed per genotype.

Scale bar: 10 μm

Genotypes: control (*MHC-Gal4/+), MHC>GluRIIA*$^{M/R}$ (*UAS- GluRIIA*$^{M/R}$*/+; MHC-Gal4/+)*

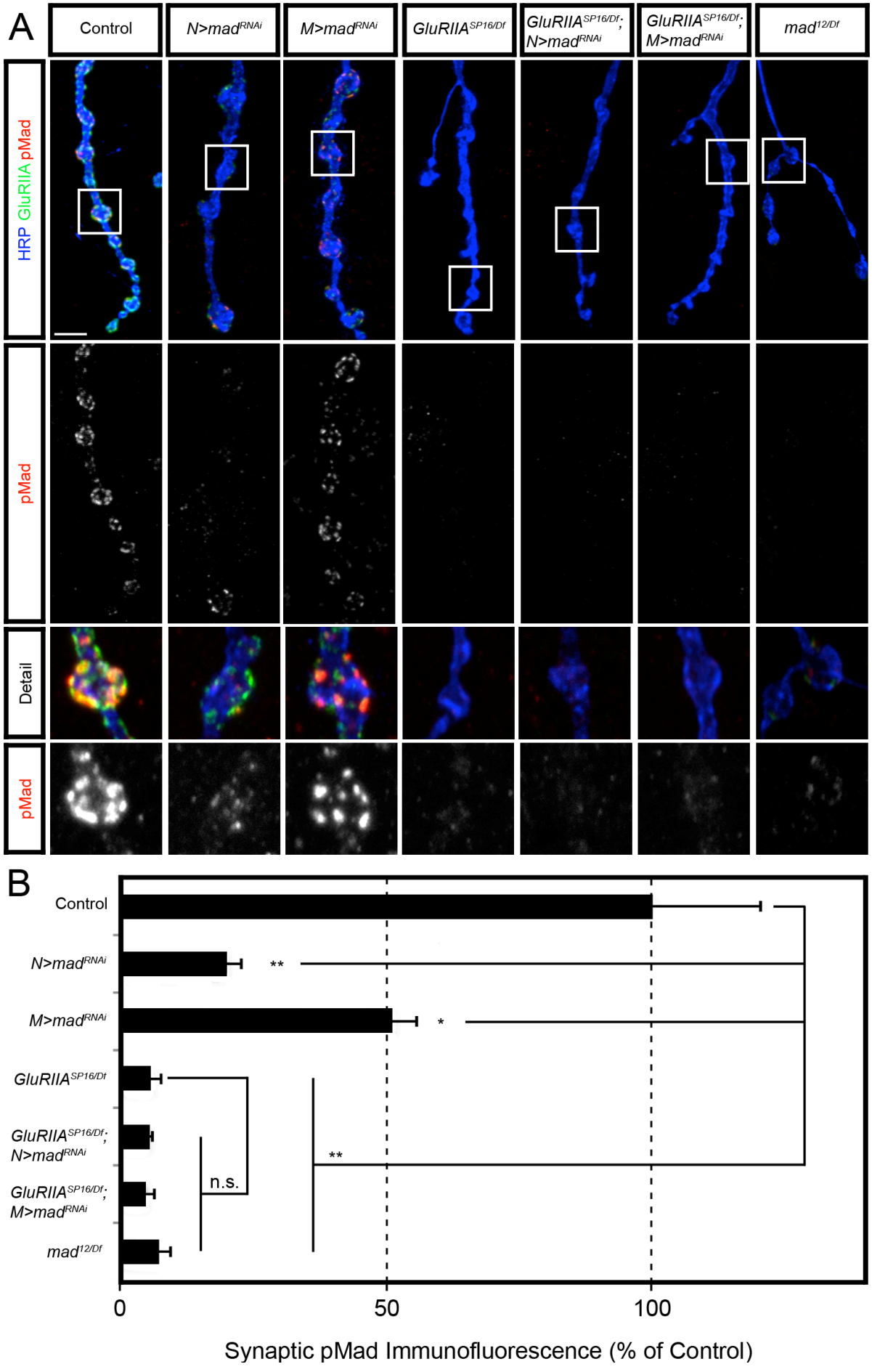
A
Control
N>mad^RNAi
M>mad^RNAi
GluRIIA^SP16/Df
GluRIIA^SP16/Df; N>mad^RNAi
GluRIIA^SP16/Df; M>mad^RNAi
mad^12/Df
HRP GluRIIA pMad
pMad
Detail
pMad
B
Control
N>mad^RNAi
M>mad^RNAi
GluRIIA^SP16/Df
GluRIIA^SP16/Df; N>mad^RNAi
GluRIIA^SP16/Df; M>mad^RNAi
mad^12/Df
**
*
**
n.s.
0
50
100
Synaptic pMad Immunofluorescence (% of Control)

**Fig. S10. The synaptic pMad signals are effectively eliminated in GluRIIA mutants.**
(A) Representative confocal images of muscle 4 NMJ, abdominal segment 3, stained for HRP (blue), GluRIIA (green) and pMad (red). Synaptic pMad is reduced by 50% when when *mad* is knocked down in the striated muscle and by 80% when *mad* is knocked down in the motor neurons. *GluRIIA* mutants have extremely low levels of synaptic pMad, comparable to mad mutants. Further reduction of Mad levels in *GluRIIA* mutants cannot further reduce the levels of synaptic pMad. Bottom panels show high magnification of boxed area imaged with increased confocal gain to visualize extremely low levels of synaptic pMad. (B) Quantification of synaptic pMad levels in larvae of indicated genotypes. Eight segments were analyzed per genotype. Error bars represent SEM.
Scale bar: 5 μm
Genotypes: control (precise excision), *N>mad$^{RNAi}$* (*UAS-mad$^{RNAi}$/+; elav-Gal4/+*), *M>mad$^{RNAi}$* (*UAS-mad$^{RNAi}$/+; 24B-Gal4/+*), *GluRIIA$^{SP16/Df}$* (*GluRIIA$^{SP16}$/ Df(2L)cl$^{h4}$*), *GluRIIA$^{SP16/Df}$; N>mad$^{RNAi}$* (*GluRIIA$^{SP16}$/ Df(2L)cl$^{h4}$, UAS-mad$^{RNAi}$; elav-Gal4/+*), *GluRIIA$^{SP16/Df}$; M>mad$^{RNAi}$* (*GluRIIA$^{SP16}$/ Df(2L)cl$^{h4}$, UAS-mad$^{RNAi}$; 24B-Gal4/+*), *mad$^{12/Df}$* (*mad$^{12}$/ Df(2L)C28*).